Korean Chem. Eng. Res., 53(1), 91-102 (2015)
http://dx.doi.org/10.9713/kcer.2015.53.1.91
PISSN 0304-128X, EISSN 2233-9558

Analysis of Forced Convection Heat Transfer for Axial Annular Flow of Giesekus Viscoelastic Fluid

Mehdi Moayed Mohseni*, Fariborz Rashidi*,† and Mohammad Reza Khorsand Movagar**

**Chemical Engineering Department, Amirkabir University of Technology, No. 472, Hafez Ave., Tehran 15875-4413, Iran*
***Petroleum Engineering Department, Amirkabir University of Technology, No. 472, Hafez Ave., Tehran 15875-4413, Iran*
(Received 21 April 2014; Received in revised form 2 July 2014; accepted 23 July 2014)

Abstract – Analytical solutions for the forced convection heat transfer of viscoelastic fluids obeying the Giesekus model are obtained in a concentric annulus under laminar flow for both thermal and hydrodynamic fully developed conditions. Boundary conditions are assumed to be (a) constant fluxes at the walls and (b) constant temperature at the walls. Temperature profiles and Nusselt numbers are derived from dimensionless energy equation. Subsequently, effects of elasticity, mobility parameter and viscous dissipation are discussed. Results show that by increasing elasticity, Nusselt number increases. However, this trend is reversed for constant wall temperature when viscous dissipation is weak. By increasing viscous dissipation, the Nusselt number decreases for the constant flux and increases for the constant wall temperature. For the wall cooling case, when the viscous dissipation exceeds a critical value, the generated heat overcomes the heat which is removed at the walls, and fluid heats up longitudinally.

Key words: Viscoelastic Fluid, Giesekus Model, Elasticity, Viscous Dissipation, Nusselt Number

1. Introduction

Heat transfer in the annulus has practical importance in some engineering applications such as annular heat exchangers, drilling operations, polymer and plastic extrusion and food industries. For example, in extrusion processes the knowledge of temperature distribution and rate of heat transfer is very important for quality control of the final product and avoiding the appearance of hot spots. These hot spots tend to occur because the low thermal conductivity of polymers has significant influence on non-uniformity of temperature variations.

Shah and London [1] obtained an analytical solution for forced convection of a Newtonian fluid in annular flow without considering viscous dissipation for different boundary conditions. Coelho and Pinho [2] investigated this problem considering viscous dissipation for the imposed boundary conditions of flux and temperature at the walls. Manglik and Fang [3] and Fang *et al*. [4] studied forced convection for Newtonian and non-Newtonian fluids in the concentric and eccentric annulus by using numerical methods and without viscous dissipation. Few other studies have also been carried out for Non Newtonian fluids in the concentric annulus without considering viscous dissipation [5-8]. Jambel *et al*. [9] studied the Graetz problem for power law model fluid, including the effect of viscous dissipation and axial conduction. Generally speaking, research on heat transfer of viscoelastic fluid is scant. An analytical solution has been derived for forced convection heat transfer of sPTT viscoelastic fluid in pipe and channel with constant flux boundary conditions at the walls and including viscous dissipation effect by Pinho and oliveira [10]. Coelho *et al*. [11] investigated the same problem with constant temperature boundary conditions. Hashemabadi *et al*. [12,13] derived an exact solution for heat transfer of sPTT model between parallel plates accounting the effect of viscous dissipation. In the aforementioned study, one of the plates was stationary and was subjected to a constant heat flux and constant temperature. The other plate moved with constant velocity and was insulated. Coelho *et al*. [14] numerically solved the Graetz problem inside pipe and channel in the presence of viscous dissipation with sPTT model for both constant heat flux and constant temperature boundary conditions at the walls and fixed inlet temperature. Oliveira *et al*. [15], in a similar research, studied this problem for FENE-P model by employing a semi-analytical method. Convective heat transfer of viscoelastic fluid inside a concentric annulus for axial flow was studied analytically by Pinho and Coelho [16] using sPTT model. Their study includes the effect of wall heating and viscous dissipation for both constant wall heat flux and constant wall temperature boundary conditions.

Khatibi *et al.* [17] presented a theoretical analysis for a Giesekus viscoelastic fluid in pipe and channel. Their study included the effect of viscous dissipation, and the boundary condition was constant heat flux at the wall.

The present study is an analytical solution of forced convection heat transfer for axial annular flow of a Giesekus viscoelastic fluid. The governing equations are simplified and solved using both isothermal and isoflux boundary conditions in the presence of viscous dissipation. Subsequently, effects of elasticity, mobility parameter

† To whom correspondence should be addressed.
E-mail: rashidi@aut.ac.ir

and viscous dissipation on the temperature distribution and Nusselt number are discussed for both heating and cooling of the walls. The details of this model have been presented by Giesekus [18,19].

2. Governing Equation

The problem is considered to be steady, laminar and fully developed both thermally and hydrodynamically. The no-slip condition exists at the walls. Axial heat conduction is neglected compared to the heat transfer in radial direction from the order of magnitude analysis [20], but the effect of viscous dissipation is included due to high viscosity of viscoelastic fluids and large velocity gradients which exist in industrial flows. Thermophysical properties of fluid are taken as constant and no dependence on temperature is considered, because it may be assumed that temperature variations will not be high enough to impose significant changes in fluid properties.

The annulus is shown schematically in Fig. 1. R_i and R_o are inner and outer cylinder radiuses, respectively. The annular gap is defined as $\delta=R_o-R_i$. and k is the radius ratio (R_i/R_o).

The Giesekus constitutive equation (without retardation time) is as follows:

$$\tau+\frac{\alpha\lambda}{\eta}(\tau\cdot\tau)+\lambda\frac{\vartheta\tau}{\vartheta t}=2\eta\dot{\gamma} \tag{1}$$

where

$$\dot{\gamma}=\frac{1}{2}[\nabla u+(\nabla u)^T] \tag{2}$$

$$\frac{\vartheta\tau}{\vartheta t}=\frac{D\tau}{Dt}-[\tau\cdot\nabla u+(\nabla u)^T\cdot\tau] \tag{3}$$

$$\frac{D\tau}{Dt}=\frac{\partial\tau}{\partial t}+(u\cdot\nabla)\tau \tag{4}$$

where τ is the stress tensor; η and λ are the model parameters representing zero shear viscosity and zero shear relaxation time, respectively [19]. The parameter α in Eq. 1 is the mobility factor and the term containing α in the constitutive equation is attributed to anisotropic Brownian motion and/or anisotropic hydrodynamic drag on the constituent polymer molecules [21]; it is required that $0\le\alpha\le1$ as discussed in [18].

The hydrodynamic solution for this flow was derived in a previous study by the authors [22]. Equations 5, 6, 7 are shear rate, shear stress and velocity profile, respectively.

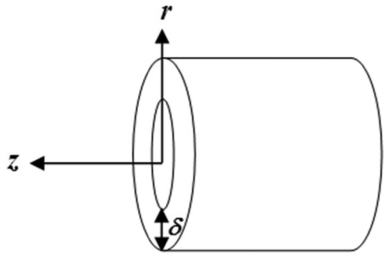

Fig. 1. Schematic view of an annular duct.

$$\gamma_{rz}^{\circ *}=\frac{1+(2\alpha-1)De\tau_{rr}^{*}}{(1+De\tau_{rr}^{*})^2}\tau_{rz}^{*} \tag{5}$$

$$\tau_{rz}^{*}=\frac{-\psi R_m^{*}}{2}\left(\frac{R_m^{*}}{r}-\frac{r}{R_m^{*}}\right) \tag{6}$$

$$u^{*}=V^{*}\Big|_{R_i^{*}}^{r^{*}} \tag{7}$$

$$V^{*}=-\frac{1}{4}\psi[v_1^{*}+v_2^{*}+v_3^{*}]$$

$$v_1^{*}=\frac{8(\alpha-1)[A-Br^{*2}]}{D[AC+DCr^{*4}-(2r^{*2}B+(1-C)^2-2)]}$$

$$v_2^{*}=\frac{(R_m^{*2}+A(2\alpha-1))\left[Ln\frac{Dr^{*2}-(1-\sqrt{C})^2}{(1+\sqrt{C})^2-Dr^{*2}}\right]}{C^{\frac{3}{2}}}$$

$$v_3^{*}=\frac{(2\alpha-1)}{D\sqrt{C}}$$

$$\{(1+\sqrt{C})^2Ln[(1+\sqrt{C})^2-Dr^{*2}]-Ln[Dr^{*2}-(1-\sqrt{C})^2](1-\sqrt{C})^2\}$$

where

$$A:R_m^{*4}De^2\alpha\psi^2\quad B:4+3R_m^{*2}De^2\alpha\psi^2\quad C:1+R_m^{*2}De^2\alpha\psi^2$$

$$D:De^2\alpha\psi^2$$

De is the Deborah number and is defined as ($De=\lambda U/\delta$), which is related to the level of elasticity, ψ is the dimensionless group for pressure gradient and R_m^{*} refers to the radius where the velocity is maximum or $\gamma_{rz}^{\circ *}=0$.

The steady state energy equation in concentric annulus for axial flow with viscous dissipation, constant thermophysical properties and negligible axial heat conduction can be represented by the following equation:

$$\rho c_p u\frac{\partial T}{\partial z}=\frac{k}{r}\frac{\partial}{\partial r}\left(r\frac{\partial T}{\partial r}\right)+\Phi \tag{8}$$

where k, ρ and c_p are thermal conductivity, density and specific heat capacity of the fluid, respectively. T is the temperature and Φ is the dissipation function, which includes only the shear stress and shear rate for this flow.

$$\Phi=\tau_{zr}\frac{\partial u}{\partial r} \tag{9}$$

Two types of boundary conditions are considered for the energy equation:

1. Constant heat fluxes at the walls:

$$r=R_i\quad -k\frac{\partial T}{\partial r}=q_i \tag{10a}$$

$$r=R_o\quad k\frac{\partial T}{\partial r}=q_o \tag{10b}$$

2. Constant temperatures at the walls:

$$r=R_i\quad T=T_i \tag{11a}$$

$$r=R_o\quad T=T_o \tag{11b}$$

3. Analytical solution

3-1. Constant heat flux boundary conditions

The following relation holds for the thermally fully developed flow [23]:

$$\frac{\partial}{\partial z}\left(\frac{T_w - T}{T_w - T_b}\right) = 0 \tag{12}$$

For the special case of constant wall heat flux, Eq. 12 reduces to:

$$\frac{\partial T}{\partial z} = \frac{\partial T_w}{\partial z} = \frac{\partial T_b}{\partial z} \tag{13}$$

T_w and T_b are wall and bulk temperatures, respectively.

Applying an energy balance over an infinitesimal element of fluid, dz, the following equation is obtained for fluid bulk temperature gradient in axial direction.

$$\frac{\partial T_b}{\partial z} = \frac{2}{m^{\circ} c_p}\left[q_i R_i + q_o R_o + \int_{R_i}^{R_o} r\tau_{zr}\frac{\partial u_z}{\partial r}dr\right] \tag{14}$$

By combining Eqs. (8), (13) and (14) and employing dimensionless terms, the following equation is obtained.

$$\frac{1}{r^*}\frac{\partial}{\partial r^*}\left(r^*\frac{\partial \Theta}{\partial r^*}\right) = X u^* - Br\Phi^* \tag{15}$$

where

$$X = 1 + \frac{2Br\int_{R_i^*}^{R_o^*} r^*\tau^*\frac{\partial u^*}{\partial r^*}dr^*}{(R_o^{*2} - R_i^{*2})} \tag{16a}$$

$$\Phi^* = \tau^*\frac{du^*}{dr^*} \tag{16b}$$

Details regarding *X* are presented in the Appendix.

The dimensionless terms are as follows:

$$u^* = \frac{u}{U} \qquad r^* = \frac{r}{\delta} \qquad \tau^* = \frac{\tau}{\eta U/\delta}$$

U is the average velocity over cross-section of the annulus.

Θ is dimensionless temperature and *Br* is the dimensionless Brinkman number, which is a measure of importance of the viscous dissipation term.

$$\Theta = \frac{k(T - T_b)}{2\delta q^{\circ}} \tag{17}$$

$$Br = \frac{\eta U^2}{2\delta q^{\circ}} \tag{18}$$

q° is the perimeter-averaged wall heat flux and is defined as follows:

$$q^{\circ} = \frac{q_i R_i + q_o R_o}{R_i + R_o} = q_i\frac{R_i + \varphi R_o}{R_i + R_o} \tag{19}$$

where φ is the ratio of outer and inner wall heat fluxes, $\varphi = q_o/q_i$.

Dimensionless thermal boundary conditions will be as follows:

$$\frac{\partial \Theta}{\partial r^*} = -\frac{1}{2}\frac{R_i^* + R_o^*}{R_i^* + \varphi R_o^*} \qquad r^* = R_i^* \tag{20a}$$

$$\frac{\partial \Theta}{\partial r^*} = \frac{\varphi}{2}\frac{R_i^* + R_o^*}{R_i^* + \varphi R_o^*} \qquad r^* = R_o^* \tag{20b}$$

Dimensionless temperature profile (Θ) can be obtained by integrating Eq. 15.

$$\Theta = X\overline{U} - Br\overline{\Phi} + C_1 Ln(r^*) + C_2 \tag{21}$$

$$\overline{U} = \int\frac{1}{r^*}\int u^* r^* dr^* dr^* \tag{22a}$$

$$\overline{\Phi} = \int\frac{1}{r^*}\int \Phi^* r^* dr^* dr^* \tag{22b}$$

Mathematical expressions for $\overline{U}$ and $\overline{\Phi}$ are presented in the Appendix.

Since both boundary conditions are of second type, determination of C_2 value is not possible directly. Hence, C_2 is eliminated from Eq. 21 by subtracting dimensionless wall temperatures (Θ_i and Θ_o) from dimensionless temperature profile (Θ) as shown below.

$$\Theta - \Theta_i = X(\overline{U} - \overline{U}|_{R_i^*}) - Br\left(\overline{\Phi} - \overline{\Phi}|_{R_i^*}\right) + C_1 Ln\left(\frac{r^*}{R_i^*}\right) \tag{23a}$$

$$\Theta - \Theta_o = X(\overline{U} - \overline{U}|_{R_o^*}) - Br\left(\overline{\Phi} - \overline{\Phi}|_{R_o^*}\right) + C_1 Ln\left(\frac{r^*}{R_o^*}\right) \tag{23b}$$

C_1 can now be obtained by applying the dimensionless boundary conditions (Eqs. 20a and 20b) as follows:

$$C_1 = R_i\left[Br\frac{d\overline{\Phi}}{dr^*}\bigg|_{r^* = R_i^*} - X\frac{d\overline{U}}{dr^*}\bigg|_{r^* = R_i^*} - \frac{1}{2}\frac{R_i^* + R_o^*}{R_i^* + \varphi R_o^*}\right] \tag{24a}$$

or

$$C_1 = R_o\left[Br\frac{d\overline{\Phi}}{dr^*}\bigg|_{r^* = R_o^*} - X\frac{d\overline{U}}{dr^*}\bigg|_{r^* = R_o^*} + \frac{\varphi}{2}\frac{R_i^* + R_o^*}{R_i^* + \varphi R_o^*}\right] \tag{24b}$$

Mathematical expressions for $d\overline{U}/dr^*$ and $d\overline{\Phi}/dr^*$ are reported in the Appendix.

Dimensionless wall temperatures are determined by using the bulk temperature definition.

$$T_b = \frac{\int_{R_i}^{R_o} 2\pi r u T dr}{\int_{R_i}^{R_o} 2\pi r u dr} \tag{25}$$

By substitution of temperature (T) from Eq. 17 into Eq. 25 and applying some mathematical manipulation, the following expressions for dimensionless wall temperatures are obtained:

$$\Theta_i = \frac{2(R_o^* - R_i^*)}{R_o^* + R_i^*}\int_{R_i^*}^{R_o^*} r^* u^*(\Theta_i - \Theta)dr^* \tag{26a}$$

$$\Theta_o = \frac{2(R_o^* - R_i^*)}{R_o^* + R_i^*}\int_{R_i^*}^{R_o^*} r^* u^*(\Theta_o - \Theta)dr^* \tag{26b}$$

Analytical solution methods to evaluate integral Eqs. 26 do not seem to be possible. Therefore, a commercial software based on

the Gauss-Kronrod numerical method was used to determine these values. The convective heat transfer from walls to the fluid is quantified by Nusselt number at inner (Nu_i) and outer walls (Nu_o). Based on the hydraulic diameter (D_H=2δ), the Nusselt number is defined as (Nu=2δh/k). The heat transfer coefficient (h) in the walls is obtained from (q_w=h(T_w-T_b)). By using dimensionless temperature definition (Eq. 17), the Nusselt number becomes ($Nu=q_w/q^o\Theta_w$) and after substituting q^o from Eq. 19, the following expressions are obtained for inner and outer Nusselt numbers.

$$Nu_i = \frac{R_i^* + R_o^*}{R_i^* + \varphi R_o^*}\frac{1}{\Theta_i} \tag{27a}$$

$$Nu_o = \frac{\varphi(R_i^* + R_o^*)}{R_i^* + \varphi R_o^*}\frac{1}{\Theta_o} \tag{27b}$$

3-2. Constant wall temperature boundary conditions

Two normalized temperatures are defined for different and identical temperatures in the walls.

$$T^* = \frac{T - T_i}{T_o - T_i} \quad \text{when} \quad T_i \neq T_o \tag{28a}$$

$$T^* = \frac{T - T_{in}}{T_w - T_{in}} \quad \text{when} \quad T_w = T_i = T_o \tag{28b}$$

Viscoelastic fluids usually have high viscosity and therefore low Reynolds number such that the advection term (u ∂T/∂z) in the energy equation can be neglected.

Substituting dimensionless terms in Eq. 8, results in the following equation:

$$\frac{1}{r^*}\frac{\partial}{\partial r^*}\left(r^*\frac{\partial T^*}{\partial r^*}\right) + Br\Phi^* = 0 \tag{29}$$

The boundary conditions and corresponding Brinkman numbers are listed below:

(1) $T_i \neq T_o$

$$T_i^* = 0 \quad \text{at} \quad r^* = R_i^* \tag{30a}$$

$$T_i^* = 1 \quad \text{at} \quad r^* = R_o^* \tag{30b}$$

$$Br = \frac{\eta U^2}{K(T_o - T_i)} \tag{31}$$

(2) $T_w = T_i = T_o$

$$T_i^* = 1 \quad \text{at} \quad r^* = R_i^* \tag{32a}$$

$$T_o^* = 1 \quad \text{at} \quad r^* = R_o^* \tag{32b}$$

$$Br = \frac{\eta U^2}{K(T_w - T_{in})} \tag{33}$$

where T_{in} is the inlet temperature.

By integrating Eq. 29 the dimensionless temperature profile will be as follows:

$$T^* = -Br\overline{\Phi} + C_1 Ln(r^*) + C_2 \tag{34}$$

C_1 and C_2 can be obtained by using Eqs. 30 for different wall temperature boundary conditions and Eqs. 32 for identical wall temperature boundary conditions.

Nusselt numbers for the two walls are derived as follows:

(1) $T_i \neq T_o$

$$Nu_i = \frac{2\left.\frac{\partial T^*}{\partial r^*}\right|_{R_i^*}}{T_b^*} \tag{35a}$$

$$Nu_o = \frac{2\left.\frac{\partial T^*}{\partial r^*}\right|_{R_o^*}}{1 - T_b^*} \tag{35b}$$

(2) $T_w = T_i = T_o$

$$Nu_i = \frac{-2\left.\frac{\partial T^*}{\partial r^*}\right|_{R_i^*}}{1 - T_b^*} \tag{36a}$$

$$Nu_o = \frac{2\left.\frac{\partial T^*}{\partial r^*}\right|_{R_o^*}}{1 - T_b^*} \tag{36b}$$

T_b^* is dimensionless bulk temperature which is determined as follows:

$$T_b^* = \frac{2}{R_o^{*2} - R_i^{*2}}\int r^* u^* T^* dr^* \tag{37}$$

The same commercial software that has been mentioned in section 3.1 was employed to obtain T_b^*.

4. Validation

If α and De in the Giesekus equation are set as zero, the model will become Newtonian. Therefore, it is expected that by choosing very small values for α and De, the results obtained for viscoelastic fluid will be similar to those of a Newtonian fluid. In this way, one can verify the accuracy of obtained equations for viscoelastic fluid.

Tables 1 and 2 compare Nu_i values obtained from Coelho and Pinho [2] study with Newtonian fluid and this study for Newtonian

Table 1. Comparison of Nu_i for Newtonian and Viscoelastic fluids from current study and [2] for constant heat flux boundary conditions at φ=1

Br	Coelho and Pinho Newtonian	This Work	
		Newtonian	α=0.05 De=0.01
0	13.1109	13.1109	13.112
0.1	6.49568	6.49567	6.49703
0.5	2.15215	2.15214	2.15277
1	1.17229	1.17229	1.17265
2	0.613575	0.613574	0.61377
5	0.252521	0.25252	0.252603

Table 2. Comparison of Nu_i for Newtonian and Viscoelastic fluids from current study and [2] for constant temperature boundary conditions and $T_i \neq T_o$

Br	Coelho and Pinho Newtonian	This Work	
		Newtonian	α=0.05 De=0.01
0	4.88897	4.88896	4.888
0.1	6.59769	6.59771	6.59735
0.5	10.9107	10.9109	10.9102
1	13.6866	13.6868	13.6863
2	16.3216	16.3219	16.322
5	18.8263	18.8266	18.8277

fluid and viscoelastic fluid with α=0.05 and De=0.01 for constant fluxes and constant temperatures at the walls, respectively, with various Br values. Results confirm the accuracy of obtained results in this study.

5. Results and Discussion

5-1. Constant heat flux boundary conditions

In the presence of viscous dissipation ($Br \neq 0$), results show different behavior for heating (Br>0) or cooling (Br<0) processes, but in the absence of viscous dissipation (Br = 0), results are independent of heating or cooling.

Although the solution presented in this study is applicable for all values of φ, only three different situations corresponding to φ=0.001, φ =1, φ=1000 are chosen for analysis.

• φ=0.001, in this case, the outer wall heat flux is much lower than the heat flux at the inner wall and, therefore, fluid thermal behavior is similar to that of an insulated outer wall.

• φ=1000 is opposite of the previous case. The outer wall heat flux is much higher than the inner wall heat flux and the fluid thermal behavior is similar to an insulated inner wall's.

• φ=1, in this case, heat fluxes at both walls are equally important.

5-1-1. Wall heating

Fig. 2 shows the effect of Brinkman number and fluid elasticity on the inner wall Nusselt number for the three selected φ values. It is seen that, by increasing Deborah number the Nusselt increases for the following reasons:

1. By increasing fluid elasticity level, the velocity profile gradient as well as fluid flow rate increase adjacent to the walls [21], and therefore, resistance to heat transfer from walls to fluid decreases.

2. Due to fluid shear-thinning behavior, when Deborah number increases, the internal heat produced by fluid viscosity decreases. Thus, the difference between wall temperature and fluid bulk temperature decreases, and according to the Nusselt number and dimensionless temperature expressions (Eqs. 27 and 17), the Nusselt number increases.

Fig. 2 also shows noticeable effects of viscous dissipation on convective heat transfer. The Nusselt number decreases when Brinkman number increases, because by increasing Brinkman the inside heat generation by viscous dissipation increases. This behavior is stronger near the walls and is expected because, according to the viscous dissipation function (Eq. 9), both shear stress and velocity gradient attain their maximum values adjacent the walls. Therefore, the difference between wall temperature and bulk temperature increases and as a result the Nusselt number decreases. The trend of Nusselt number is different for φ=1000 (Fig. 2c). In this case, Nusselt is negative for low Brinkman numbers, while it is positive for high Brinkman numbers with a singularity in the Nusselt curve. Thus, at low Brinkman numbers the inner wall temperature is lower than the bulk temperature, which is due to insulating circumstances at the inner wall, and therefore, Nusselt becomes negative. But, by increasing Brinkman due to the higher heat generation near the wall, the difference between bulk temperature and wall temperature reduces until it tends to zero, and as a result Nusselt number approaches infinity. If the Brinkman number increases even more, the inner wall temperature will be higher than bulk temperature and as a result Nusselt becomes positive.

Effects of Deborah number and mobility factor (α) on the inner wall Nusselt number are shown in Fig. 3, for different values of Brinkman numbers. The elasticity level of fluid is directly proportional to the value of mobility factor. This is because the mobility factor can be indirectly related to the concentration of the polymer: i.e., α=0 represents dilute solutions, while α=0.5 represents high concentrated solutions [24]. Hence, the effect of α on heat transfer is

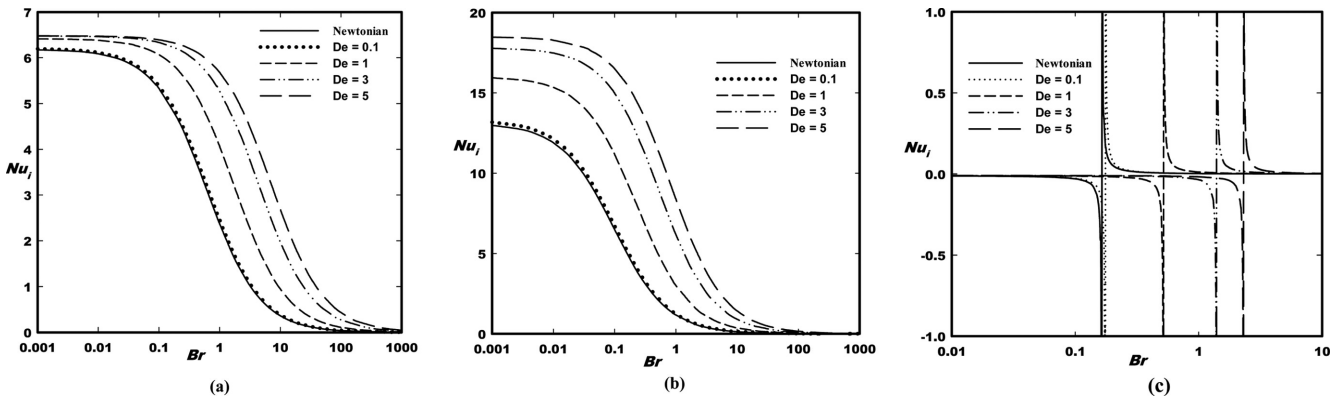

Fig. 2. Variation of Nu_i with positive Br and De for α=0.1, κ=0.5 (a) φ=0.001 (b) φ=1 (c) φ=1000.

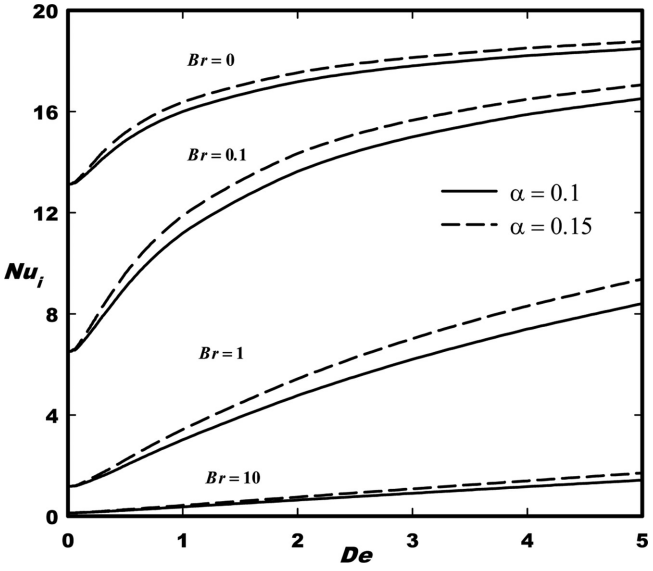

Fig. 3. Variation of Nu_i versus De for different positive Br at α=0.1 and α=0.15 for κ=0.5 and φ=1.

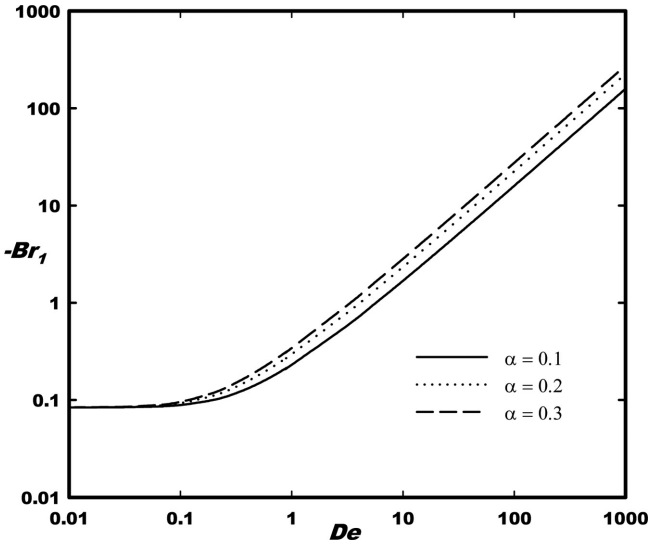

Fig. 5. Effects of α and De on the first critical Brinkman number variation.

similar to the effect of De. This is evident from Fig. 3.

According to Fig. 4a and Fig. 4b, by increasing De and α, i.e., higher elasticity, the difference between wall temperature and fluid temperature decreases, which is due to having higher heat transfer at high elasticity (see Fig. 2 and Fig. 3). By increasing Br, the difference between wall temperature and fluid temperature increases (Fig. 4c), which has already been discussed.

Also, the behavior of the outer wall Nusselt number is similar to the behavior of inner wall Nusselt number but for reversed heat flux ratios: Nu_o varies monotonically for φ=1000 and exhibits singularities for φ=0.001, and at φ=1, both Nusselt numbers show similar behavior.

5-1-2. Wall cooling

Wall cooling (q^o<0) is applied to reduce the bulk temperature of fluid. In this process viscous dissipation plays a more important role than it does in the heating process, and the strength of viscous dissipation might change the overall heat balance. For small absolute values of Brinkman number, negative heat flux in the walls reduces the bulk temperature of fluid in the axial direction ($\partial T/\partial Z$<0), but as the absolute Brinkman number becomes larger than a critical value, the internal heat produced by viscous dissipation overcomes the effect of wall cooling and fluid starts to warm up itself ($\partial T/\partial Z$>0). This critical value is called the first critical Brinkman number (Br_1), and is determined by putting Eq. 14 equal to zero.

$$Br_1 = \frac{-1}{2\int_{R_i^*}^{R_o^*} r^* \tau^* \frac{\partial u^*}{\partial r^*} dr^*} \Big/ (R_i^* + R_o^*) \tag{38}$$

Fig. 5 shows the effect of Deborah number and mobility factor on the first critical Brinkman number. It is seen that, by increasing De and α, absolute value of Br_1 increases, which means that cooling range of fluid is being extended. So, by increasing fluid elasticity there is no need to impose large heat fluxes for the cooling process to occur. This effect is related to the shear thinning behavior of fluid where, by increasing fluid elasticity the viscosity of fluid and consequently the heat internally generated by viscous

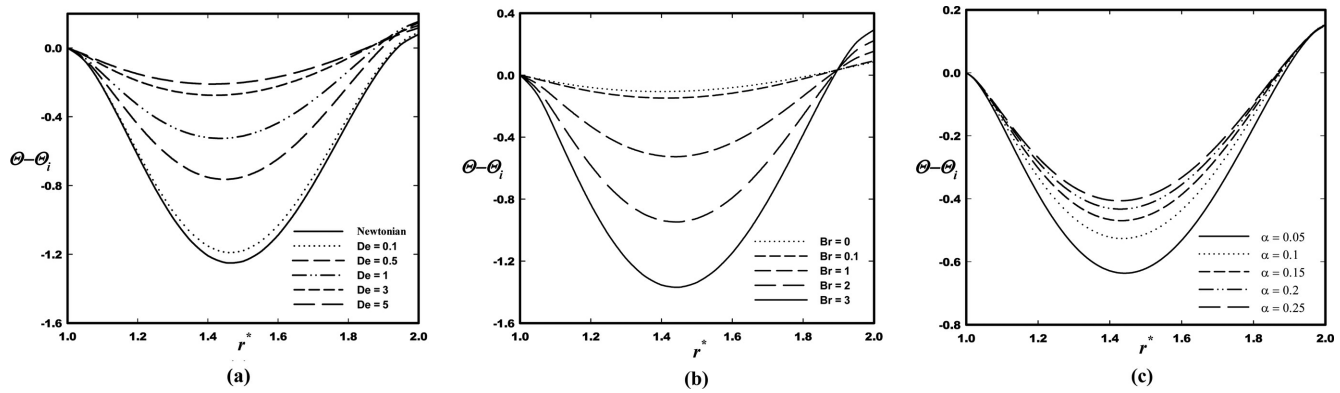

Fig. 4. Dimensionless temperature profile with variation (a) De at Br=1 and α=0.1 (b) a at Br=1 and De=1 (c) Br at De=1 and α=0.1, for κ=0.5 and φ=1.

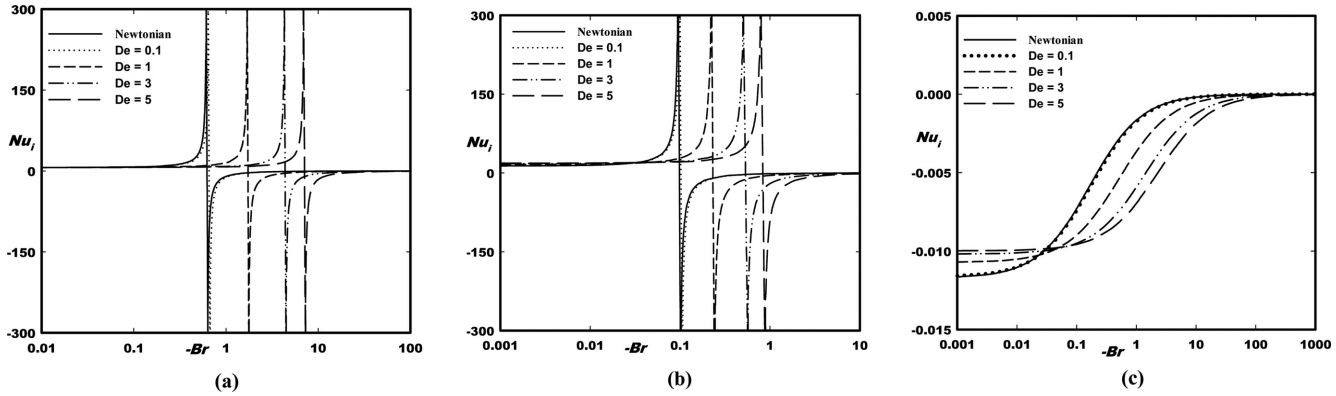

Fig. 6. Variation of Nu_i versus negative Br and De for α=0.1, κ=0.5 (a) φ=0.001 (b) φ=1 (c) φ=1000.

dissipation decreases, and therefore the cooling range of fluid extends.

For Brinkman number larger than the first critical Brinkman ($|Br|>|Br_1|$), a second critical Brinkman number (Br_2) appears and Nusselt number approaches to infinity. In other words, a singularity occurs in the Nusselt curve. As can be seen from Fig. 6, when $|Br|<|Br_2|$ the Nusselt number is positive and increases by increasing Brinkman. Considering negative heat flux in the walls, it is expected that wall temperatures to be lower than fluid bulk temperature; and since the flux sign is also negative, the Nusselt number will be positive. As heat generated due to viscous dissipation increases, the difference between bulk temperature and wall temperature decreases and subsequently Nusselt number increases. At the second critical Brinkman number, wall temperature reaches to bulk temperature, and thus the Nusselt number approaches infinity. For $|Br|>|Br_2|$, the wall temperature becomes higher than the bulk temperature and the sign of the Nusselt number changes. In addition, by further increase of Brinkman number, the difference between wall temperature and bulk temperature increases and Nusselt number approaches to zero. The effects of Deborah on Nusselt number can be divided into two parts:

1. For $|Br|<|Br_2|$, wall temperature is lower than bulk temperature. Since the fluid elasticity reduces the effect of viscous dissipation due to shear thinning behavior of fluid, by increasing Deborah number, the difference between wall temperature and bulk temperature increases and consequently Nusselt number decreases.

2. For $|Br|>|Br_2|$, wall temperature is higher than bulk temperature and any increase in Deborah number decreases the difference between wall temperature and bulk temperature and therefore, Nusselt number increases.

In Fig. 6c which is related to φ=1000, there is no singularity point, and variation of Nu_i versus Br is monotonic and Nusselt number is negative for all Brinkman values. This was expected, because in this case inner wall temperature is always higher than bulk temperature due to the output heat flux which is dominant at the outer wall. Also by increasing Brinkman, Nusselt decreases, because the difference between wall temperature and bulk temperature increases. The effect of fluid elasticity on Nusselt number is complicated. In fact, coupling of elasticity and viscous dissipation results in opposite behaviors in high and low values of Brinkman numbers. For high values of Brinkman, increasing the fluid elasticity increases Nusselt number. However, when viscous dissipation is weak this trend will be reversed and Nusselt decreases by increasing fluid elasticity. This behavior is also evident in Fig. 7, which represents the effects of De, α and Br on Nusselt curve.

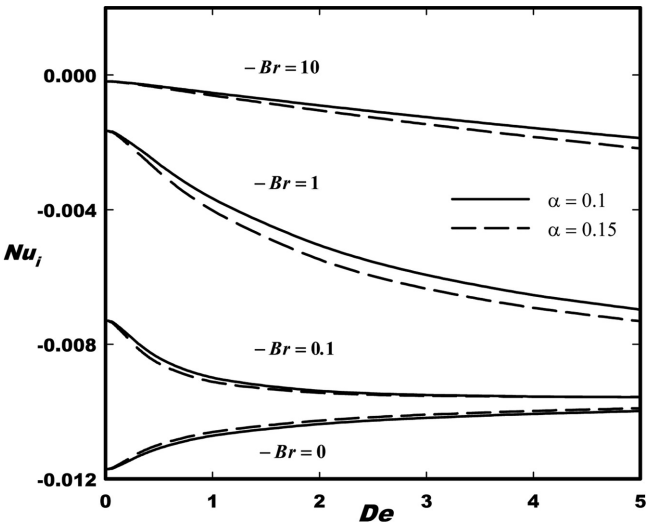

Fig. 7. Variation of Nu_i versus De for different negative Br at α=0.1 and α=0.15 for κ=0.5 and φ=1.

5-2. Constant wall temperature boundary conditions

For the different wall temperatures case, if the outer wall temperature is higher than the inner wall temperature ($T_o>T_i$), Brinkman number is positive (Br>0) and if ($T_o<T_i$), then Brinkman number is Negative (Br<0).

Fig. 8 presents the effects of Brinkman and Deborah numbers on dimensionless temperature distribution. The upper parts of diagrams are related to Br>0, and the lower parts are related to Br<0. The upper and the lower parts show similar behaviors but in a mirror-symmetrical fashion. This means that the trend of changes for the positive Brinkman numbers in the region close to the inner wall is similar to the trend of the changes for the negative Brinkman num-

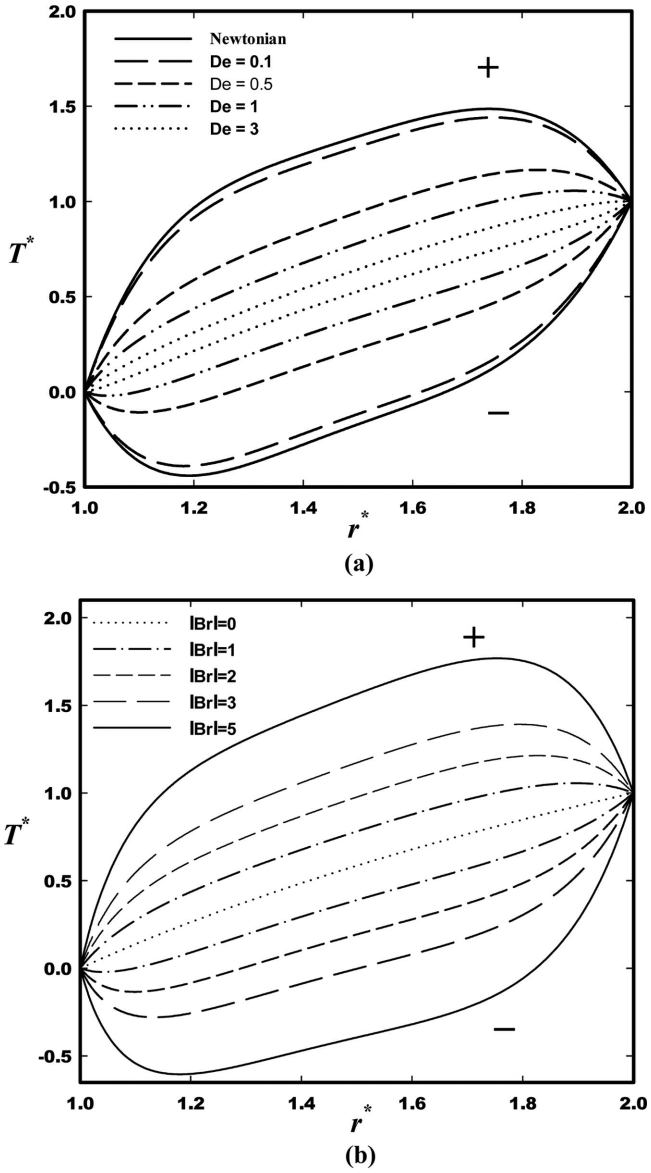

Fig. 8. Dimensionless temperature profile with variations of (a) De and |Br|=1 (b) |Br| and De=1, for α=0.1, κ=0.5 and $T_i \neq T_o$.

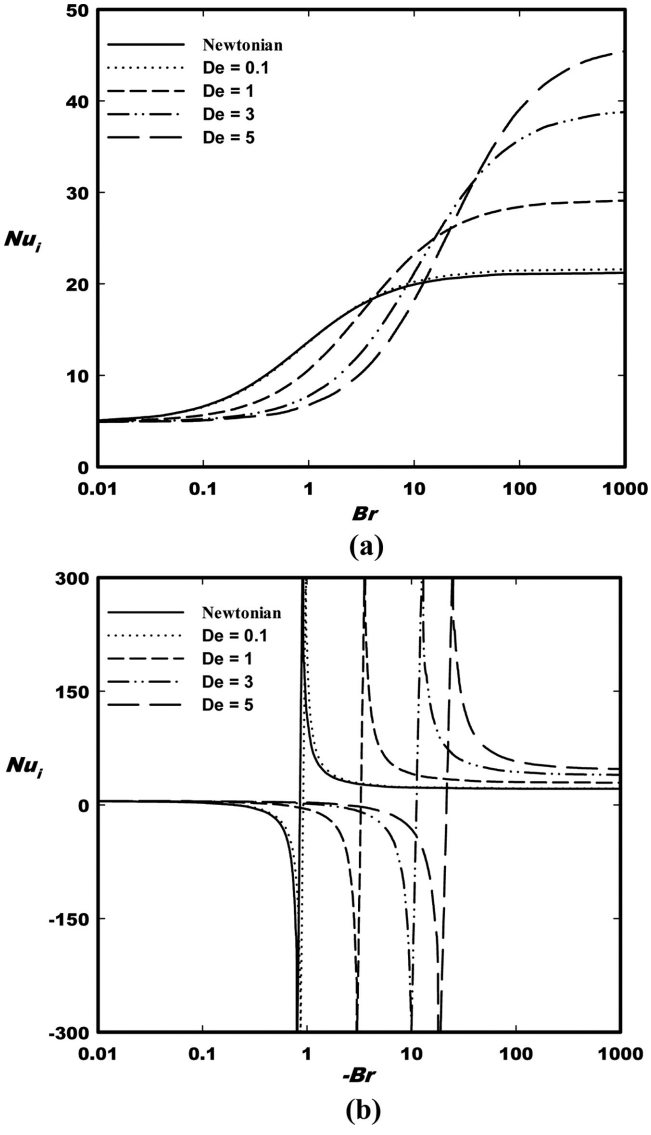

Fig. 9. Variation of Nu_i with De and (a) Br>0 (b) Br<0 for α=0.1, κ=0.5 and $T_i \neq T_o$.

bers in the region close to the outer wall and vice versa.

As can be seen from this figure, the effect of increasing Brinkman and Deborah on temperature profile is opposite of one another, because by increasing Brinkman the heat internally generated by viscous dissipation increases, but when the elasticity level increases due to shear-thinning behavior of fluid, the inside heat generation decreases. For small values of viscous dissipation the fluid starts to heat up with uniform slope from the colder wall until it reaches to the temperature of the warmer wall. But by increasing Brinkman number, the temperature reaches a maximum value near the warmer wall. Subsequently, direction of heat flux changes and in fact a cooling process happens at the warmer wall. This behavior is due to the heat internally generated by viscous dissipation, which increases fluid temperature. But, since the boundary conditions are set as fixed temperatures at the walls, the fluid temperature will be higher than warmer wall temperature, and therefore the fluid will be cooled at the both walls.

Fig. 9 shows effects of Brinkman and Deborah on inner Nusselt number. Fig. 9a and Fig. 9b are related to positive and negative Brinkman numbers, respectively. In Fig. 9a by increasing Brinkman number, the Nusselt number increases due to stronger viscous dissipation, generating more internal heat to be evacuated, which leads to higher Nusselt numbers. But when viscous dissipation is coupled with elasticity, opposite behaviors are observed for small and large Brinkman numbers. For small Brinkman numbers, an increase in elasticity causes decrease in Nusselt, but for large Brinkman numbers increasing elasticity increases Nusselt number. This can be clarified by referring to Fig. 8a, where, by increasing elasticity temperature, the gradient at the inner wall (wall heat flux) is decreased. Also, because of sharper velocity gradient adjacent to the walls for high elasticity and hence reduction of thermal resistance, the difference between the bulk temperature and wall temperature is decreased. As for normal-

ized temperature expression, the dimensionless bulk temperature is also decreased. For small Brinkman numbers, the decrease in wall heat flux due to elasticity growth is higher than the decrease in dimensionless bulk temperature; as a result, the Nusselt number is reduced, but this behavior is reversed at higher values of Brinkman.

Note that for positive Brinkman numbers the minimum temperature occurs at the inner wall, so the normalized bulk temperature is always positive. Also, the temperature gradient is positive at the inner wall. Thus, according to Eq. 35a, the Nusselt number should also be positive, and in this case Nusselt curve is always monotonic. But for negative Brinkman numbers a singularity point happens in the Nusselt curve (Fig. 9b). For small Brinkman numbers, since wall heat flux and normalized bulk temperature are both positive, the Nusselt number will be positive. But by increasing viscous dissipation, Nusselt drops to zero and then becomes negative. This occurrence is related to cooling phenomenon at the warmer wall, which causes the temperature gradient to become zero and then negative as already discussed. Also by Brinkman growth, bulk temperature increases, but since wall temperature is constant, the difference between these temperatures is reduced until it tends to zero and as a result singularity occurs in Nusselt curve. For higher values of Brinkman the bulk temperature will be higher than the wall temperature, and therefore the sign of Nusselt will be changed again.

Fig. 10 shows the effect of Deborah number and mobility factor on Nusselt curve for positive values of Brinkman number. Similar behavior as Fig. 9a is observed when elasticity effects are coupled to viscous dissipation effects.

For the identical wall temperature case, as can be seen in Fig. 11, Nusselt number increases by increasing fluid elasticity level, but it is independent of Brinkman number. Note although, by changing Brinkman number, both dimensionless temperature gradient and normalized bulk temperature vary; however, their variations are such that the ratio of numerator to denominator of Nusselt fraction (Eqs. 36) is kept constant.

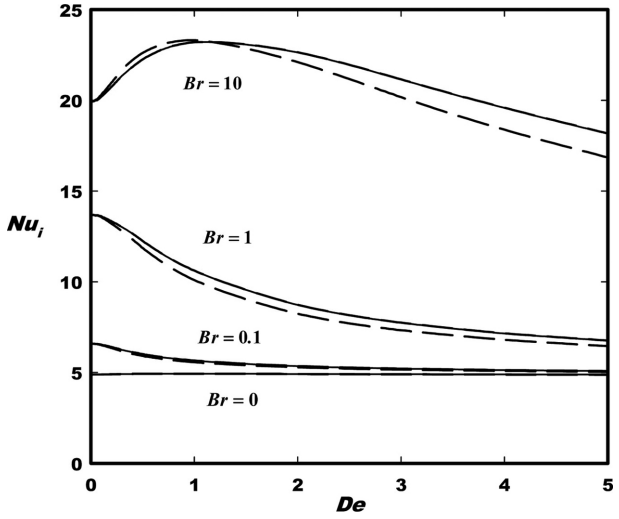

Fig. 10. Variation of Nu_i versus De for different positive Br at α=0.1 and α=0.15 for κ=0.5 and $T_i \neq T_o$.

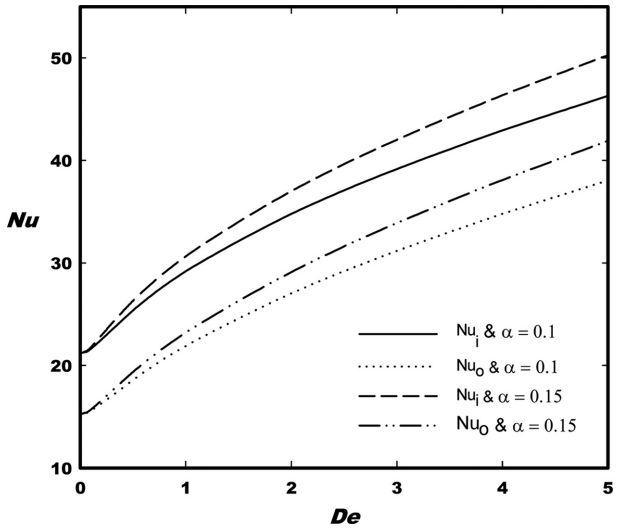

Fig. 11. Variation of Nu_i and Nu_o with De and α for κ=0.5 and T_i=T_o.

6. Conclusions

Forced convection heat transfer in the concentric annulus was investigated by the analytical method for viscoelastic fluid obeying Giesekus model. The problem was analyzed under steady, laminar, thermal and hydrodynamical fully developed conditions and including viscous dissipation. Thermo-physical properties were assumed independent of temperature and axial heat conduction was negligible. Boundary conditions were constant wall heat fluxes and constant wall temperatures. Brinkman and Nusselt numbers, which are presented as dimensionless groups to show the importance of viscous dissipation and convective heat transfer level respectively, were defined for two cases of boundary conditions. Effects of viscous dissipation along with elasticity (Deborah dimensionless group and mobility factor), were investigated on Nusselt number and dimensionless temperature profile. Results showed a significant influence of these parameters on heat transfer. For the constant flux boundary conditions, analysis was also performed for fluid heating (Br > 0) and fluid cooling (Br < 0). In the cooling process a critical Brinkman number (Br_1) is derived. When Brinkman number becomes larger than this critical value, heat generated internally by viscous dissipation overcomes the effect of wall cooling and fluid starts to warm up. For the constant temperature boundary conditions, two cases of different and identical wall temperatures were considered. It was shown that when walls temperatures are identical, Nusselt number is independent of viscous dissipation.

Nomenclatures

Br : Brinkman number
C_1 : first integration constant
C_2 : second integration constant
c_p : specific heat at constant pressure (J/kg.K)
De : Deborah number, De=λU/δ

D_H : hydraulic diameter, $D_H \equiv 2\delta$
h : heat transfer coefficient (Watt/m^2.K)
k : thermal conductivity (Watt/m.K)
Nu : Nusselt number, $Nu=2h\delta/k$
q : heat flux (Watt/m^2)
r : radial coordinate (m)
R_i : radius of inner cylinder
R_o : radius of outer cylinder
R_m : radius where velocity is maximum
t : time (s)
T : fluid temperature (K)
u : velocity (m/s)
U : average velocity
z : axial coordinate (m)

Greek Letters

α : mobility factor
δ : annular gap, $\delta=R_o-R_i$
$\dot{\gamma}$: shear rate tensor (s^{-1})
η : zero-shear viscosity (Pa.s)
λ : zero-shear relaxation time (s)
ρ : fluid density (kg/m^3)
τ : stress tensor (Pa)
ψ : dimensionless group for pressure gradient
κ : radius ratio
φ : ratio of outer and inner wall heat fluxes
Φ : viscous dissipation function
Θ : dimensionless temperature for isoflux boundary conditions
ϑ : convected derivative

Subscripts

w : refers to wall value
b : refers to bulk value
in : refers to inlet
i : refers to inner wall
o : refers to outer wall

Superscripts

* : refers to dimensionless quantities
T : transpose of tensor

References

1. Shah, R. K. and London, A. L., *Laminar Flow Forced Convection in Ducts*, Academic Press, New York(1978).
2. Coelho, P. M. and Pinho, F. T., *Int. J. Heat Mass Transfer*, **49**, 3349(2006).
3. Manglik, R. M. and Fang, P., *Int. J. Heat Fluid Flow*, **16**, 298 (1995).
4. Fang P., Manglik, R. M. and Jog, M. A., *J. Non-Newton. Fluid Mech*., **84**, 1(1999).
5. Raju, K. K. and Devanathan, R., *Rheol. Acta*., **10**, 484(1971).
6. Hong, S. N. and Matthews, J. C., *Int. J. Heat Mass Transfer*, **12**, 1699(1969).
7. Batra, R. L. and Sudarsan, V. R., *Comput. Meth. Appl. Mech. Eng*., **95**, 1(1992).
8. Tanaka, M. and Mitsuishi, N., *Heat Transfer Jpn. Res*., **4**, 26(1975).
9. Jambal, O., Shigechi, T., Davaa, G. and Momoki, S., *Int. Comm. Heat Mass Transfer*, **32**, 1174(2005).
10. Pinho, F. T. and Oliveira, P. J., *Int. J. Heat Mass Transfer*, **43**, 2273(2000).
11. Coelho, P. M., Pinho, F. T. and Oliveira, P. J., *Int. J. Heat Mass Transfer*, **45**, 1413(2002).
12. Hashemabadi, S. H., Etemad, S. Gh., Narenji, M. R. G. and Thibault, J., *Int. Commun. Heat Mass Transfer*, **30**, 197(2003).
13. Hashemabadi, S. H., Etemad, S. Gh. and Thibault, J., *Int. J. Heat Mass Transfer*, **47**, 3985(2004).
14. Coelho, P. M., Pinho, F. T. and Oliveira, P. J., *Int. J. Heat Mass Transfer*, **46**, 3865(2003).
15. Oliveira, P. J., Coelho, P. M. and Pinho, F. T., *J. Non-Newton. Fluid Mech*., **121**, 69(2004).
16. Pinho, F. T. and Coelho, P. M., *J. Non-Newton. Fluid Mech*., **138**, 7(2006).
17. Khatibi, A. M., Mirzazadeh, M. and Rashidi, F., *Heat Mass Transfer*, **46**, 405(2010).
18. Giesekus, H., *J. Non-Newton. Fluid Mech*., **11**, 69(1982) .
19. Giesekus, H., *J. Non-Newton. Fluid Mech*., **12**, 367(1983).
20. Kakac, S. and Yener, Y., *Convective Heat Transfer*, CRC Press (1995).
21. Bird, R. B., Amstrong, R. C. and Hassager, O., *Dynamics of Polymeric Liquids: Fluid Mechanics*, Vol. 1, Wiley, New York(1977).
22. Mohseni, M. M. and Rashidi, F., *J. Non-Newton. Fluid Mech*., **165**, 1550(2010).
23. Bejan, A., *Convection Heat Transfer*, Wiley, New York(1995).
24. Bhatara, G., Shaqfeh, E. S. G. and Khomami, B., *J. Rheol*., **49**, 929(2005).

Appendix

$$a = 1+C+2\sqrt{C}$$

$$\bar{a} = -1-C+2\sqrt{C}$$

$$m = 1+2C-C^2$$

$$H = \frac{D}{\psi}$$

$$F_1 = \frac{R_m^{*2}+A(2\alpha-1)}{C\sqrt{C}}$$

$$F_2 = \frac{2\alpha-1}{D\sqrt{C}}$$

$$F_3 = aF_2 - F_1$$

$$\overline{F_3} = \bar{a}F_2 + F_1$$

$$F_4 = \sqrt{1+B^2+4C-4C^3+C^4-2Bm+2C^2-C^2AD}$$

$$F_5 = 1-B+2C-C^2$$

$$F_6 = -\frac{4(B^2-ACD+B(-m+F_4))(\alpha-1)}{CD^2F_4}$$

$$\overline{F_6} = \frac{4(B^2-ACD-B(m+F_4))(\alpha-1)}{CD^2F_4}$$

$$F_7 = -\frac{aF_3}{D}$$

$$\overline{F_7} = \frac{\bar{a}\overline{F_3}}{D}$$

$$F_8 = D(AC+R_i^{*2}(2-2B+4C-2C^2+CDR_i^{*2}))$$

$$F_9 = 8(1-\alpha)(BR_i^{*2}-A)+8DF_2R_i^{*2}\sqrt{C}F_5+4C\sqrt{C}DF_2(A+DR_i^{*4})$$

$$F_{10} = ACDF_1+2DF_1R_i^{*2}F_5+D^2F_1R_i^{*4}C$$

$$F_{11} = 0.5\left(F_1-\overline{F_3}-\frac{F_{10}}{F_8}-\frac{F_9}{F_8}-F_3-\frac{F_{10}}{F_8}Ln\left(\frac{\bar{a}+DR_i^{*2}}{a-DR_i^{*2}}\right)\right)$$

$$F_{12} = \frac{0.5a}{D}\left(F_1-\frac{F_{10}}{F_8}-F_3\right)$$

$$F_{13} = F_7Ln|a|+\overline{F}_7Ln|\bar{a}|+F_6Ln|F_4-F_5|+\overline{F}_6Ln|F_4+F_5|$$

$$F_{14} = \frac{1}{2}\left(\frac{F_{10}}{F_8}+F_3\right)$$

$$F_{15} = 0.5(\overline{F}_3-F_1)$$

$$F_{16} = 1+C^2-R_m^{*4}D^2$$

$$F_{17} = \sqrt{1+2C+C^2-R_m^{*4}D^2}$$

$$F_{18} = \frac{R_m^{*4}(\alpha-1)\psi^2}{C\sqrt{C}}$$

$$F_{19} = \frac{4\alpha-3}{H^2\sqrt{C}}$$

$$F_{20} = \frac{1-2\alpha}{2\alpha De^2}$$

$$F_{21} = \frac{4(1+C)(\alpha-1)}{CH^2}$$

$$F_{22} = \frac{(F_{17}-F_{16}+C(6+F_{17}))(\alpha-1)}{CH^2F_{17}}$$

$$\overline{F}_{22} = \frac{(F_{17}+F_{16}+C(-6+F_{17}))(\alpha-1)}{CH^2F_{17}}$$

$$F_{23} = 1+C+F_{17}$$

$$\overline{F}_{23} = -1-C+F_{17}$$

$$F_{24} = -4R_m^{*4}D(1+C)(\alpha-1)$$

$$F_{25} = 4(8C+R_m^{*4}D^2)(\alpha-1)$$

$$F_{26} = F_{18}-aF_{19}$$

$$\overline{F}_{26} = F_{18}+\bar{a}F_{19}$$

$$F_{27} = R_m^{*4}D-2(1+C)R_o^{*2}+R_o^{*4}D$$

$$\overline{F}_{27} = R_m^{*4}D-2(1+C)R_i^{*2}+R_i^{*4}D$$

$$F_{28} = F_{20}(R_o^{*2}-R_i^{*2})+\frac{1}{2CH^2}\left(\frac{F_{24}+F_{25}R_o^{*2}}{F_{27}}-\frac{F_{24}+F_{25}R_i^{*2}}{\overline{F}_{27}}\right)$$
$$+0.5F_{26}Ln\left(\frac{a-DR_o^{*2}}{a-DR_i^{*2}}\right)-0.5\overline{F}_{26}Ln\left(\frac{\bar{a}+DR_o^{*2}}{\bar{a}+DR_i^{*2}}\right)$$

$$X = 1+\frac{2BrF_{28}}{R_o^{*2}-R_i^{*2}}$$

$$\overline{\Phi} = 0.5\begin{pmatrix} F_{20}r^{*2}-F_{21}Ln(r^*)+F_{22}Ln(F_{23}-Dr^{*2})+\overline{F}_{22}Ln(\overline{F}_{23}+Dr^{*2}) \\ +F_{26}\left(Ln(a)Ln(r^*)-0.5\ PolyLog\left[2,\frac{Dr^{*2}}{a}\right]\right) \\ -\overline{F}_{26}\left(Ln(\bar{a})Ln(r^*)-0.5\ PolyLog\left[2,-\frac{Dr^{*2}}{\bar{a}}\right]\right) \end{pmatrix}$$

$$\overline{U} = -\frac{\psi}{8}\begin{pmatrix} F_{11}r^{*2}+F_{13}Ln(r^*)+F_{12}Ln(a-Dr^{*2})+\frac{\overline{F}_3\bar{a}Ln(\bar{a}+Dr^{*2})}{2D}+ \\ r^{*2}\begin{pmatrix} 0.5F_1Ln\left(\frac{\bar{a}+Dr^{*2}}{a-Dr^{*2}}\right)+ \\ F_{14}Ln\left(\frac{a-Dr^{*2}}{a-DR_i^{*2}}\right)+F_{15}Ln\left(\frac{\bar{a}+Dr^{*2}}{\bar{a}+DR_i^{*2}}\right) \end{pmatrix} \\ -0.5\begin{pmatrix} F_7\ PolyLog\left[2,\frac{Dr^{*2}}{a}\right]+\overline{F}_7\ PolyLog\left[2,-\frac{Dr^{*2}}{\bar{a}}\right] \\ +F_6\ PolyLog\left[2,\frac{CDr^{*2}}{F_4-F_5}\right]+\overline{F}_6\ PolyLog\left[2,-\frac{CDr^{*2}}{F_4+F_5}\right] \end{pmatrix} \end{pmatrix}$$

$$\frac{d\overline{\Phi}}{dr^*} = r^*\left(F_{20}+\frac{D\overline{F}_{22}}{\overline{F}_{23}+Dr^{*2}}-\frac{DF_{22}}{F_{23}-Dr^{*2}}\right)+\left(\frac{F_{26}Ln[a-Dr^{*2}]-\overline{F}_{26}Ln[\bar{a}+Dr^{*2}]-F_{21}}{2r^*}\right)$$

$$\frac{d\overline{U}}{dr^*} = -\frac{\psi}{8}\left(\begin{array}{c} r^*\left(\begin{array}{c} 2F_{11} + \dfrac{\overline{F}_3\bar{a}}{\bar{a}+Dr^{*2}} - \dfrac{2DF_{12}}{a-Dr^{*2}} + F_1 Log\left[\dfrac{\bar{a}+Dr^{*2}}{a-Dr^{*2}}\right] + 2F_{14} Log\left[\dfrac{a-Dr^{*2}}{a-DR_i^{*2}}\right] \\ 2F_{15} Log\left[\dfrac{\bar{a}+Dr^{*2}}{\bar{a}+DR_i^{*2}}\right] \end{array}\right) + \\ \left(\begin{array}{c} \dfrac{F_7 Log\left[a-\dfrac{Dr^{*2}}{a}\right] + \overline{F}_7 Log\left[1+\dfrac{Dr^{*2}}{\bar{a}}\right] + F_6 Log\left[1-\dfrac{CDr^{*2}}{F_4-F_5}\right]}{r} \\ + \overline{F}_6 Log\left[1+\dfrac{CDr^{*2}}{F_4+F_5}\right] + F_{13} \end{array}\right) + \\ r^{*3}\left(\dfrac{2DF_{15} + F_1 D(a+\bar{a})/(a-Dr^{*2})}{\bar{a}+Dr^{*2}} - \dfrac{2DF_{14}}{a-Dr^{*2}}\right) \end{array}\right)$$

$$Br_1 = \frac{-(R_i^* + R_o^*)}{2F_{28}}$$